



## OPEN The overexpression of human amylin in pancreatic $\beta$ cells facilitate the appearance of amylin aggregates in the kidney contributing to diabetic nephropathy

S Iglesias-Fortes<sup>1</sup>, C González-Blanco<sup>1,2</sup>, A García-Carrasco<sup>3</sup>, A Izquierdo-Lahuerta<sup>3</sup>, G García<sup>1,2</sup>, A García-Aguilar<sup>1,2,4</sup>, A Lockwood<sup>1,2</sup>, O Palomino<sup>1,2,4</sup>, G Medina-Gómez<sup>3</sup>, M Benito<sup>1,2</sup> & C Guillén<sup>1,2</sup>✉

Diabetic nephropathy is one of the most frequent complications of diabetic patients and is the leading cause of end-stage renal disease worldwide. The complex physiopathology of this complication raises a challenge in the development of effective medical treatments. Therefore, a better understanding of this disease is necessary for producing more targeted therapies. In this work we propose human amylin as a possible mediator in the development of diabetic nephropathy. Islet amyloid polypeptide or amylin is a hormone co-secreted with insulin. The human isoform has the ability to fold and form amyloid aggregates in the pancreas of patients with type 2 diabetes mellitus, disrupting cellular homeostasis due to its ability to form pores in lipid bilayers. It has been described that hIAPP can be secreted and exported in extracellular vesicles outside the pancreas, being a plausible connecting mechanism between the  $\beta$ -cell and other peripheral tissues such as the kidney. Here, we demonstrate that tubular, podocytes and mesangial cells can incorporate hIAPP coming from  $\beta$ -cells. Then, this hIAPP can form aggregates inside these kidney cells, contributing to its failure. In order to study the consequences *in vivo*, we found amylin aggregates in the kidney of mice overexpressing hIAPP after feeding a high fat diet. In addition, we observed an increase in glomerulosclerosis index and inflammation. Specifically, there were significant changes in signalling pathways directly involved in the diabetic nephropathy such as an increased in mTORC1 signaling pathway, an alteration in mitochondrial dynamics and an increased in endoplasmic reticulum stress. All these results demonstrate the importance of hIAPP in the kidney and its possible contribution in the development of diabetic nephropathy.

Type 2 diabetes (T2DM) is a progressive disease that begins with an hyperactivation of pancreatic  $\beta$  cells and a hyperinsulinemia phenotype, in order to compensate insulin resistance. This situation is known as prediabetic state. However, as the disease progresses, there is a disruption of pancreatic  $\beta$  cells, and the onset of a hypoinsulinemic scenario, likely due to an increase in pancreatic  $\beta$  cell apoptosis<sup>1</sup>. It is known that throughout the progression of the disease, the mTORC1 signalling pathway is chronically activated<sup>2</sup>. This induction is necessary to facilitate pancreatic  $\beta$  cell proliferation during the first phase of the disease. However, when this activation becomes chronic, several deleterious mechanisms are induced such as endoplasmic reticulum (ER) stress (ER-stress), inhibition of the protective mechanism of autophagy as well as the ubiquitin-proteasome

<sup>1</sup>Department of Biochemistry and Molecular Biology, Faculty of Pharmacy, Complutense University of Madrid, Plaza Ramón y Cajal s/n, Ciudad Universitaria, IDISSC, Madrid 28040, Spain. <sup>2</sup>CIBER de Diabetes y Enfermedades Metabólicas Asociadas, Instituto de Salud Carlos III, Madrid 28040, Spain. <sup>3</sup>Department of Basic Sciences of Health, Area of Biochemistry and Molecular Biology, Universidad Rey Juan Carlos, Alcorcon 28922, Spain. <sup>4</sup>Department of Pharmacology, Pharmacognosy and Botany, Faculty of Pharmacy, Complutense University of Madrid, Madrid, Spain. ✉email: cguillen@ucm.es

system (UPS) and mitochondrial dysfunction<sup>2,3</sup>. Autophagy permits the degradation of different components of the cell such as aged organelles, aggregates and many others, and serves as a protective mechanism for several cell types including pancreatic  $\beta$  cells<sup>4–6</sup>. In fact, it is known that in humans, as the disease progresses, the elimination of disrupted mitochondria by a specific autophagy known as mitophagy, switches from a correct mitophagy during the pre-diabetic state towards an alteration in mitophagy in the diabetic situation<sup>7</sup>.

Amylin is a small protein that is co-secreted with insulin and it is incorporated into the same secretory granules. Amylin plays important roles in human physiology such as the induction of satiety or delaying gastric emptying<sup>8</sup>. However, amylin can form aggregates, which are associated with pancreatic  $\beta$  cell loss during the progression to T2DM<sup>9</sup>. Interestingly, not all the amylin derived from the different species are amyloidogenic. For instance, rodents present a type of amylin, which it cannot form aggregates. However, the human form is amyloidogenic and can generate  $\beta$ -sheet aggregates. This difference arises from variations in an amyloidogenic region in the primary sequence of the protein. Rodent variants of amylin present several proline residues, which are responsible for inhibiting aggregate formation and are considered as  $\beta$ -sheet breakers. In contrast, the human variant and variants in other species such as cats lack prolines in this region and can form aggregates<sup>8</sup>. The main mechanism involved in the elimination of these aggregates is autophagy, concomitantly with the UPS<sup>10,11</sup>. In our study, using the rat insulinoma pancreatic  $\beta$  cell line with an overexpression of human amylin (INS1E-hIAPP) we uncovered an increased mTORC1 signalling pathway and an altered autophagy, mitophagy and a mitochondrial pro-fission scenario, leading to an induction of ER-stress<sup>12</sup>. More recently, we have observed that INS1E-hIAPP cells possess a detoxifying mechanism, which involves the production of extracellular vesicles (EVs) containing hIAPP. Then, we exposed neuron cells with the EVs purified from INS1E-hIAPP, which induced alterations in these cells. This is important because represents a pathway for the exportation of these toxic proteins to other territories, defining a new strategy for the cell-to-cell communication<sup>13</sup>.

Kidney is one of the main tissues which is frequently affected as the disease progresses leading to the development of diabetic nephropathy (DN)<sup>14</sup>. It is known that amylin can deposit in the kidney, predisposing to hypertension, mitochondrial dysfunction and an increased formation of reactive oxygen species (ROS) and hypoxia<sup>15</sup>. In fact, it has been observed that amylin is found in biopsies derived from patients with DN. Although amylin is widely distributed, mainly was found in the mesangial area, Bowman's capsule and in blood vessels, causing glomerulosclerosis<sup>16,17</sup>. However, the molecular mechanism underlying the deposition and alteration of the kidney in diabetic patients is currently unknown.

In this study, we used a diabetic model by the overexpressing of human amylin in pancreatic  $\beta$  cells (TghIAPP) treated with a high fat diet (HFD) for either 4 months or 8 months of age. Using this model, we have determined that amylin accumulates mainly in the glomerular area, generating amylin aggregates with an increased inflammation and glomerulosclerosis index in the TghIAPP under the treatment with HFD, contributing to the appearance of DN during the progression of T2DM. In addition, we have carried out in vitro studies, adding a conditioned medium coming from INS1E-hIAPP, to three mouse renal cell lines (mouse proximal tubular (MCT), mesangial (MM) and podocytes. Interestingly, we have observed an accumulation of amylin in all of them.

## Materials and methods

### Cell lines

Mouse tubular, mesangial and podocytes were generously gifted by Adriana Izquierdo (Rey Juan Carlos University). These cells were cultured in 10% FBS RPMI 1640 medium supplemented with penicillin G (12  $\mu$ g/mL), streptomycin (10  $\mu$ g/mL), amphotericin B (0,25  $\mu$ g/mL), Mycozap<sup>TM</sup> Plus-CL (Lonza, Switzerland) and 10 mM HEPES. Rat insulinoma cell line, INS1E overexpressing human amylin (INS1E hIAPP) was generously supplied by Anna Novials (IDIBAPS, Barcelona, Spain) and described in<sup>18</sup>. INS1E-hIAPP cell lines were cultured in 10% FBS RPMI 1640 medium supplemented with 1 mM sodium pyruvate, 10 mM HEPES, 200  $\mu$ g/ml of Geneticin and the antibiotics previously mentioned.

### Mice model

FVB/N hemizygous transgenic mice were developed by Jackson Laboratory (Strain No. 008232)<sup>19</sup>. According to the description of the model, these mice express human amylin (hIAPP) under the rat insulin II promoter. Besides, hIAPP RNA is observed in pancreas, kidney, and stomach, but hIAPP protein is reported only in pancreas tissues. In this study only heterozygous male mice were used due to homozygous die around 16 weeks of age, presenting a severe genotype. In order to minimize the contribution of the different genetic backgrounds, we decided to obtain the heterozygous in a mixed background by crossing FVB/N hemizygous transgenic mice with C57BL/6 Wt mice for at least 6 generations. Tg and Wt mice were fed with either standard (STD) or high fat diet (HFD) during 4 or 8 months. The HFD was obtained from Envigo and 60% of the calories were obtained from fat. In order to check that the mice were gaining weight, they were weighed every week and tested for glucose and insulin tolerance. All animal experimentation described was conducted according to accepted standards of human-animal care, as approved by the animal experimentation institutional committee (PROEX number 112.2/21). All the methods are reported in accordance with ARRIVE guidelines. All experiments were performed in accordance with relevant guidelines and regulations. The animals were euthanized using a mixture of xilacine (150 mg/Kg) and ketamine (50 mg/Kg).

### Antibodies and reagents

Anti-Drp1 (#8570S) and anti-phospho Drp1 (S616) (#3455S) were obtained from Cell Signaling Technology (Beverly, MA). Anti-Amylin (ab55411), anti-mfn1 (ab104274), anti-mfn2 (ab56889) were from Abcam. Anti-Bip (#3177), anti-p70 (#9202) and anti p-p70 (#2211) were from Cell Signaling Technology. Secondary antibodies

HRP-conjugated used: anti-Rabbit (NA934) and anti-Mouse (NA931) were obtained from GE Lifesciences. MG5 is a fluorescent styrylquinoline that is capable to detect  $\beta$ -sheet aggregates as it was originally described<sup>20</sup>.

### Western blotting

Tissues were removed and homogenized in a lysis buffer [Nonidet-P40 1% (v/v), Tris-HCl 50mM, EDTA 5mM, EGTA 5mM, NaCl 150mM, NaF 20mM, pH 7.5, PMSF 1mM, aprotinin 10  $\mu$ g/ml, leupeptin 2  $\mu$ g/ml and sodium orthovanadate 1mM) with a Polytron homogenizer. Subsequently, each sample was sonicated and centrifuged at 13,000 rpm for 15 min. Protein concentration determination was achieved by the Bradford dye method, using de Bio-Rad<sup>®</sup> (Hercules, CA) reagent. Equal amounts of protein were submitted to electrophoresis and after SDS-PAGE gels were transferred to Immobilon PVDF membranes (Merck Millipore, Burlington, MA) following the Western Blot wet transfer protocol. Then, membranes were blocked and incubated overnight with primary antibodies at 4 °C at the concentration recommended by the manufacturer. The next day, the membranes were washed with TTBS and incubated at room temperature with the corresponding secondary antibodies diluted in TTBS. After, the secondary antibody was removed and three washes were performed with TTBS. The corresponding bands were visualized using the ECL Western blotting protocol (GE Healthcare, Little Chalfont, UK).

### Immunofluorescence

Cells were grown on glass coverslips and fixed using paraformaldehyde 4% solution during 20 min, permeabilized in PBS with 0,5% Triton X-100 for 15 min, and then blocked with blockage solution (3% BSA, 0,1% Tween 20 in PBS) for 1 h. Then MG5, the organic compound was diluted in DMSO to 10  $\mu$ M, and cells were incubated with the solution during 30 min before DAPI staining (1  $\mu$ g/ml) for 10 min.

### Red Congo and IAPP immunohistochemistry

The first step is a deparaffinization process consisting of a 15-minute xylene run and a battery of alcohols (100%, 96%, 90%, and 70% ethanol) for 4 min each. Subsequently, 10 min with Congo Red solution (0.2% Congo Red, 70% isopropanol, and 30% distilled water). Finally, it was washed with 70% isopropanol for 2 min and with distilled water for 1 min. From this step the immunohistochemistry protocol was started. For IAPP immunohistochemistry, kidney sections from all mice groups were incubated with rabbit polyclonal IAPP antibody (ab55411) at 1/100 in PBS-Tween/1% bovine serum antigen overnight at 4°C. Then, a secondary antibody incubation and development using a diaminobenzidine substrate kit was performed. All images were taken at 20X magnification and amylin staining was measured using ImageJ software.

### MCP-1, A11 and caspase-1 immunohistochemistry

Fixed renal tissue Sect. (4  $\mu$ m) were dehydrated and then embedded in paraffin. The sections were deparaffinized, rehydrated and incubated with primary antibody MCP-1 (Santa Cruz Biotechnology, Inc.), A11 (AHB0052) and caspase-1 (sc-56036). Sections were incubated with a biotinylated anti-IgG (Vector Laboratories) and incubated with the avidin-biotin-peroxidase complex (Vector Laboratories), 3,3'-diaminobenzidine (DAB) substrate (Merck, Germany) was used as the chromogen. The tissue sections were counterstained with Harris haematoxylin. Some kidney samples were incubated without primary antibody as negative controls. The stained renal tissue sections were imaged with a light microscope Zeiss Standard 25. To four slides per animal were quantified ( $n=4$  animals/group), and not consecutive slides were taken. Image J 1.45 software (National Institutes of Health, Bethesda, MD, USA) were used.

### PAS staining

Kidney sections were deparaffinized by passing them through xylene, alcohols of decreasing concentration and, subsequently, through distilled water. For staining with Schiff's reagent, a commercial kit (130802, BioOptica, Milan, Italy) was used. The sections were counterstained with hematoxylin, specifically included in the kit. After this, the tissue sections were dehydrated with increasing concentrations of alcohol and xylene. Finally, they were covered with DePex mounting medium (Serva). Glomerular images were digitized using a Canon Powershot A640 camera attached to a light microscope Zeiss Standard 25. Sections were scored semiquantitatively in a blinded manner by two independent observers: staining intensity negative (0), mild (1+), moderate (2+) or strong (3+). The final score was the mean of the two evaluations.

### Transmission electron microscopy

Kidney tissue was fixed in 2.5% glutaraldehyde, postfixed in 1% osmium tetroxide, dehydrated with an increasing concentration of ethanol and embedded in epoxy resin. Renal ultrathin sections were processed as described<sup>21</sup>. Foot process width and glomerular basement membrane thickness were measured using ImageJ software, as previously described<sup>22</sup>. All mitochondrial parameters were measured using Fiji software (National Institutes of Health). Ten measurements per kidney and four kidneys were investigated per experimental group.

### Glucose tolerance test and insulin tolerance test

Glucose tolerance test (GTT) and insulin tolerance test (ITT) were performed on mice as described elsewhere<sup>23</sup>. Briefly, for the GTTs, in overnight (16 h)-fasted mice glucose was administered (2 g/kg body weight) by i.p injection. The measurements were performed in a glucometer every 30 min using Accu-Check Aviva blood glucose strips (Roche, Penzberg, Germany). ITTs were performed in the random-fed state. The animals were injected with 1 U/kg body weight of human regular insulin (Humulin regular, Eli Lilly, Indianapolis, IN, USA) and blood glucose levels were measured at indicated times. ITT data are presented as percentage of initial blood glucose concentration.

### Statistical analysis

Statistical differences between groups were determined using One way ANOVA for Western Blot and Student's t-test for images quantifications. Differences were considered statistically significant at  $p < 0.05$  (\* $p < 0.05$ ; \*\* $p < 0.01$ ; \*\*\* $p < 0.005$ , \*\*\*\* $p < 0.0005$ ).

## Results

### Presence of hIAPP aggregates in mesangial, tubular and podocytes cells

Previous reports conducted in our laboratory had already demonstrated the ability of INS1E overexpressing human amylin (hIAPP) (INS1E-hIAPP) cells to produce extracellular vesicles containing hIAPP. These vesicles were collected in the conditioned medium (CM) of these cells, under high glucose conditions<sup>13</sup>. In order to know whether amylin could be incorporated into renal cells and facilitates its aggregation similarly to INS1E-hIAPP, different types of kidney-derived cells were exposed to the CM obtained after the incubation of INS1E-hIAPP cells with high glucose (16.7mM) for 24 h. Subsequently, the CM was added to mesangial, tubular and podocytes for 8 and 24 h. As it was previously described<sup>15</sup>, using an organic fluorescent compound (MG5)

that detects  $\beta$ -sheet aggregates, we observed that after the incubation with the CM, there was an accumulation of these aggregates in a time-dependent manner in all the kidney cell lines. This aggregation capacity was higher after 24 h (Fig. 1) in all the cell lines.

### Increase endoplasmic reticulum stress and alterations in the mTORC1 pathway in renal cells containing amylin aggregates

Following the detection of amylin aggregates, the impact on protein aggregation was assessed by examining ER stress and the mTORC1 pathway. This evaluation was conducted using conditioned medium concurrent with the detection of amylin aggregates, specifically at 8 and 24 h. Our findings revealed a noteworthy increase in PERK phosphorylation, accompanied by an elevation in the Bip chaperone levels, particularly evident at 24 h in both mesangial and tubular cells (Fig. 2B, D, E, G, I and J). Additionally, a reduction in phosphorylation levels of p70 and ULK1 at residue 757 was observed, being statistically significant at the 24-hour time point in mesangial cells (Fig. 2A and C). However, this decrease was not significant in tubular cells (Fig. 2F and H). On the other hand, no changes were found in cell death markers neither in Bcl-xL (anti-apoptotic protein) in mesangial cells nor in cleaved caspase-3 in mesangial and tubular cells (Supplemental Fig. 1A and Supplemental Fig. 1B). In podocytes, a significant increase in Bip levels was observed at 8 h, with no change in p-p70 levels (Fig. 2K, L and M). In turn, an increase in cleaved caspase-3 is observed at this time point (Supplemental Fig. 1C). This demonstrates how kidney cells respond to the presence of  $\beta$ -amyloid aggregates by regulating three interconnected pathways, which are mTORC1, endoplasmic reticulum stress and cell death.

### Renal cell lines with amylin aggregates did not exhibit significant changes in mitochondrial dynamics

Mesangial and tubular cells did not exhibit significant alterations in the dynamin-related protein 1 (Drp1) phosphorylation status or in mitofusins 1 and 2 protein levels (Mfn1 and Mfn2). Although not statistically significant, there was a reduction in Mfn1 protein levels in both cell types, being more pronounced after 24 h, although not statistically significant (Fig. 3A-3 H). However, in podocytes, there was a significant reduction in both Mfn1 and Mfn2 protein levels with no significant changes in phospho-Drp1 (Fig. 3I and L). Examination of the previous markers, allowed us to assess

that mitochondria were affected by the presence of aggregates. Reduced mitofusins indicate a fission-driven mitochondrial state, as does increased phosphorylation of DRP1.

### Accumulation of hIAPP aggregates in the kidney of a diabetic mouse under HFD

After identifying that hIAPP can be incorporated into different kidney cell lines, we wanted to analyze the relevance of this finding using a mice model with an overexpression of hIAPP in pancreatic  $\beta$  cells (TghIAPP) under a high fat diet (HFD) for the generation of an insulin resistant state. After weaning, mice were treated with HFD for either 3 months or 7 months. In 4-month-old (4 M) WT mice under a high fat diet (HFD) there was an increase in glucose intolerance. However, in the TghIAPP, under a standard diet (STD) we could observe a basal glucose intolerance that it was not worsened after the HFD (Fig. 4A). In addition, there was a concomitant increase in insulin resistance in the WT mice after HFD and in the TghIAPP in both situations (Supplemental Fig. 2A). In contrast, in 8-month-old (8 M) mice, there was a dramatic increase in glucose intolerance in the TghIAPP mice after feeding HFD (Fig. 4B), with an associated insulin resistance in this group of animals (Supplemental Fig. 2B). The levels of IAPP in the kidney were evaluated by immunohistochemistry and an increase was observed in the TghIAPP mice at both 4 months and 8 months compared to WT, regardless of their diet. Paradoxically, the levels of IAPP were lower in TghIAPP 8 M than those observed in TghIAPP 4 M mice (Fig. 4C). Similar results were obtained using western blot for amylin detection (Supplemental Fig. 3). Very importantly, when we analyzed the presence of aggregates using Congo red staining, we only detected a positive staining in the glomerulus and in the periglomerular area in the TghIAPP mice after the HFD at 8 M of age (Fig. 4C). On the other hand, oligomeric species detected by immunohistochemistry using A11 antibody were only observed in the 4 M TghIAPP mice fed with HFD. These aggregates were observed in the glomerular area (Supplemental Fig. 4A) but, mainly observed, in the tubular area (Supplemental Fig. 4B).

### Increased in both MCP-1 signal and in the glomerulosclerosis index in tg hIAPP mice

In order to assess the degree of tissue inflammation, monocyte chemoattractant protein-1 (MCP-1) levels were measured by immunohistochemistry. In this regard, it was found that both the TghIAPP mice at 4 M and 8 M, fed with a standard diet (STD), exhibited a noteworthy increase in MCP-1 levels compared to their respective

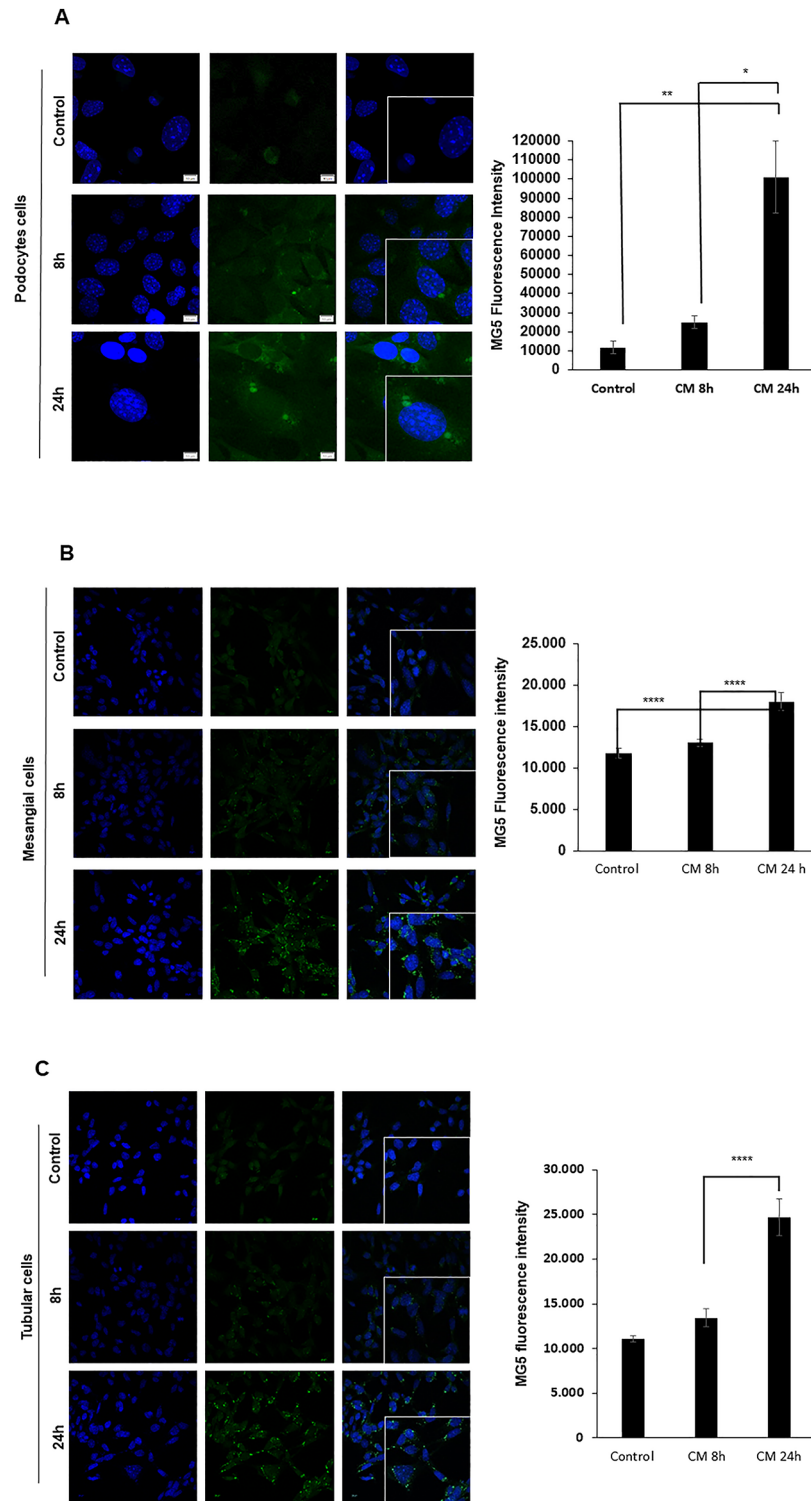


**Fig. 1.** Kidney cells present hIAPP aggregates after incubation with CM from INS1E-hIAPP during 8 and 24 h. A, B, C: Immunofluorescence staining of podocyte, mesangial and tubular cells, respectively. Aggregates were detected with MG5 compound (green signal) and cell nuclei with DAPI (blue). The plot indicates the mean and standard deviation, n (independent studies) = 3. \*  $p < 0,05$ ; \*\*  $p < 0,01$ ; \*\*\*  $p < 0,005$ ; \*\*\*\*  $p < 0,0005$ .

controls. Although no differences were found between TghIAPP 4 M and 8 M mice under HFD compared to their WT counterparts, there was a further increase in the level of MCP1 staining intensity under the treatment with the HFD compared with the STD diet (Fig. 5A and C). Glomerulosclerosis is one of the hallmarks of diabetic nephropathy and a sign of renal damage. In this regard, we found that both, under STD of HFD, the TghIAPP mice showed a significant increase in the glomerulosclerosis index compared to



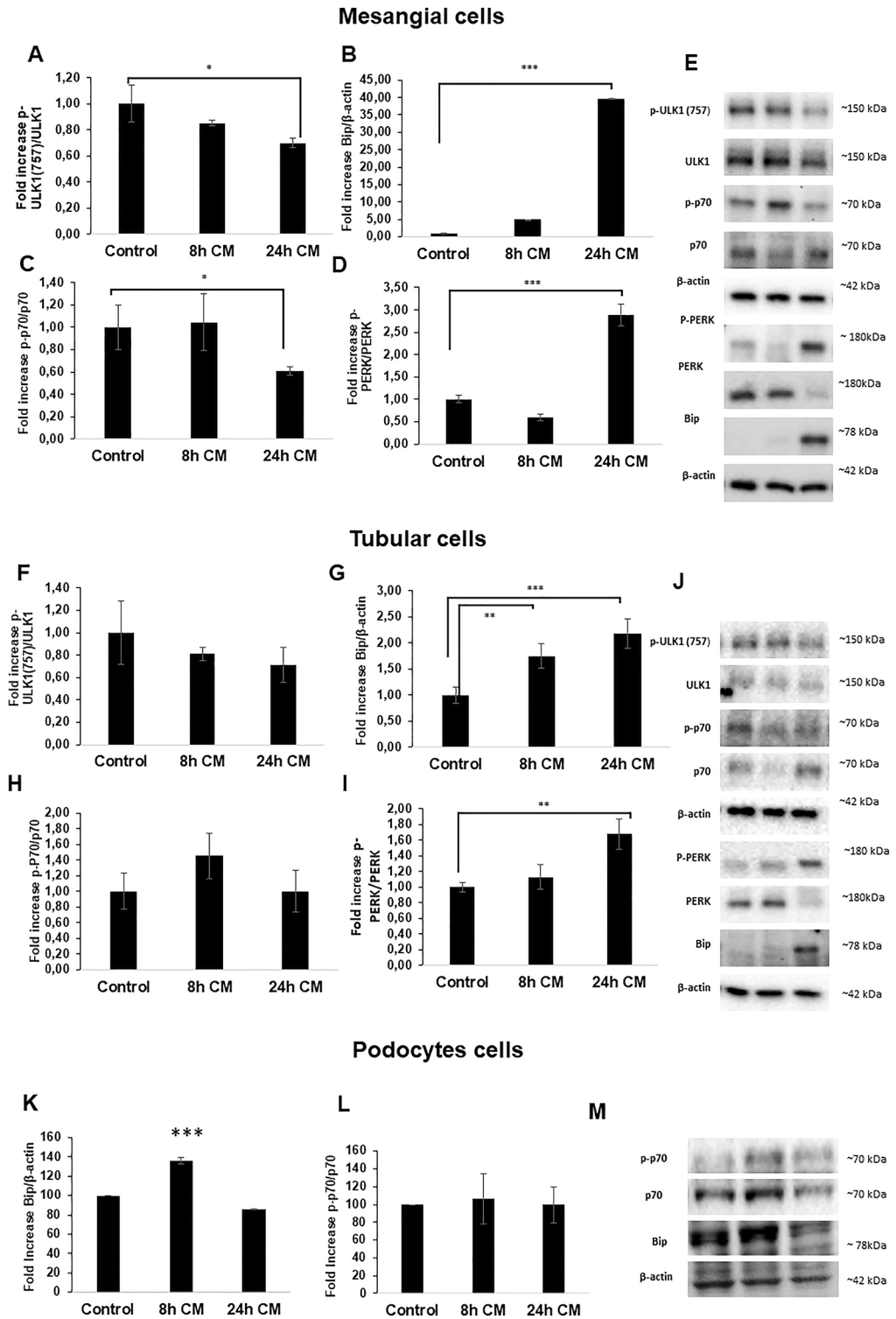


**Fig. 2.** Analysis of mTORC1 and ER pathway in kidney cells. The levels of p-ULK1(757), p-p70, Bip and p-PERK are shown, demonstrating the significance increase in ER stress. A–E: show the results in mesangial cells, F–J: tubular cells, K–M: podocytes cells. The plots indicate the mean and standard error is represented (n (independent studies) = 3–4; \*  $p < 0,05$ ; \*\*  $p < 0,01$ ; \*\*\*  $p < 0,005$ ; \*\*\*\*  $p < 0,0005$ ).

WT mice. In addition, the TgIAPP 4 M mice under HFD presented a significant increase in this index compared to the Tg 4 M STD mice. However, no major differences were observed between the Tg 8 M STD and Tg 8 M HFD mice (Fig. 5D and F). In addition, we observed the appearance of effaced foot processes in the podocytes from the TgIAPP 8 M mice under STD conditions and in both WT and TgIAPP mice under HFD by electron microscopy (Fig. 5G). To corroborate the observed increase in MCP1 protein levels, we examined the

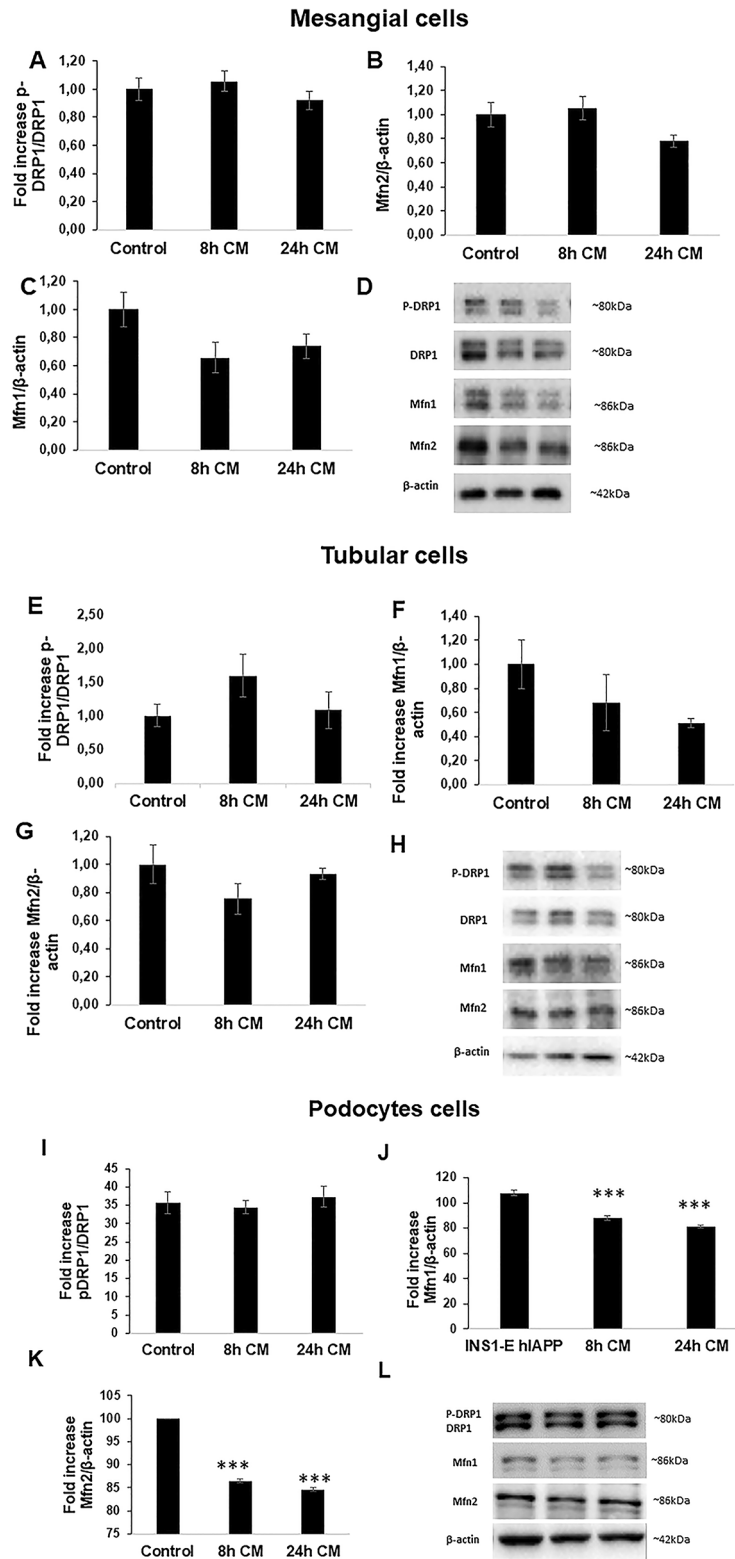


**Fig. 3.** Analysis of mitochondrial dynamics in kidney cells. The levels of p-DRP1, Mfn1 and Mfn2 are shown. The decrease in Mfn1 and Mfn2 is observed, being significant only in the case of podocytes. A-D: show the results in mesangial cells, E-H: tubular cells, I-L: podocytes cells. The plots indicate the mean and standard error is represented (n (independent studies) = 3–4; \*  $p < 0,05$ ; \*\*  $p < 0,01$ ; \*\*\*  $p < 0,005$ , \*\*\*\*  $p < 0,0005$ ).

levels of caspase-1, a protein integral to the immune response and responsible of the inflammasome signaling pathway cascade. Our analysis revealed a significant upregulation of caspase-1 expression in 8 M TghIAPP mice

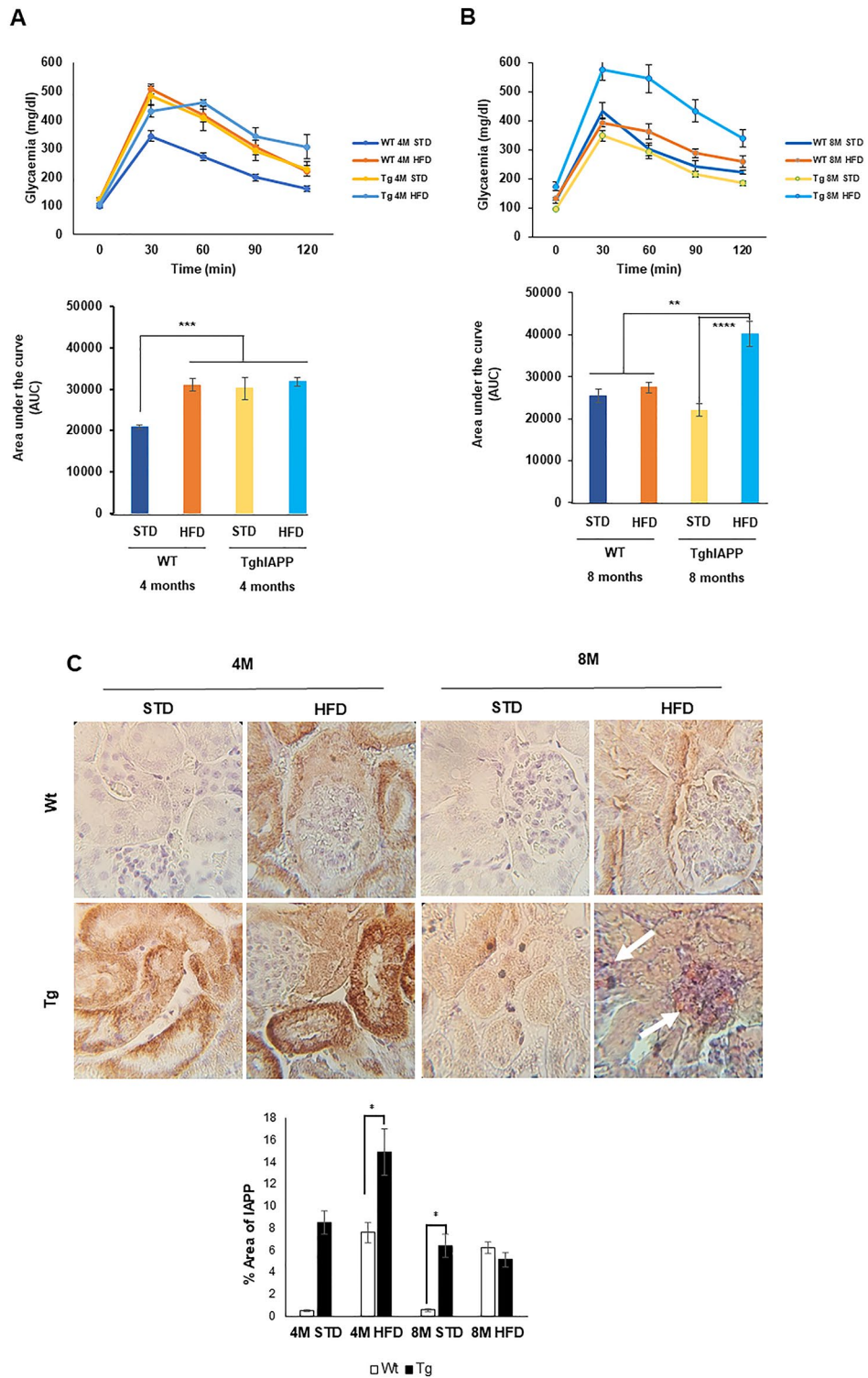


**Fig. 4.** Glycaemic profile and the levels of IAPP with the presence of hIAPP aggregates in kidney of Tg hIAPP 8 M HFD mice. **A, B:** Glucose tolerance test of 4 M and 8 M Tg hIAPP and Wt mice. **C:** Immunohistochemistry of IAPP and Congo Red staining. The plots indicate the mean and standard error (n (mice number) = 4–7). \*  $p < 0,05$ ; \*\*  $p < 0,01$ ; \*\*\*  $p < 0,005$ , \*\*\*\*  $p < 0,0005$ .

under both standard STD and HFD diets, compared to Wt mice. Furthermore, among the 8 M Tg hIAPP mice, those on the HFD exhibited the highest levels of caspase-1 (Supplemental Fig. 5).



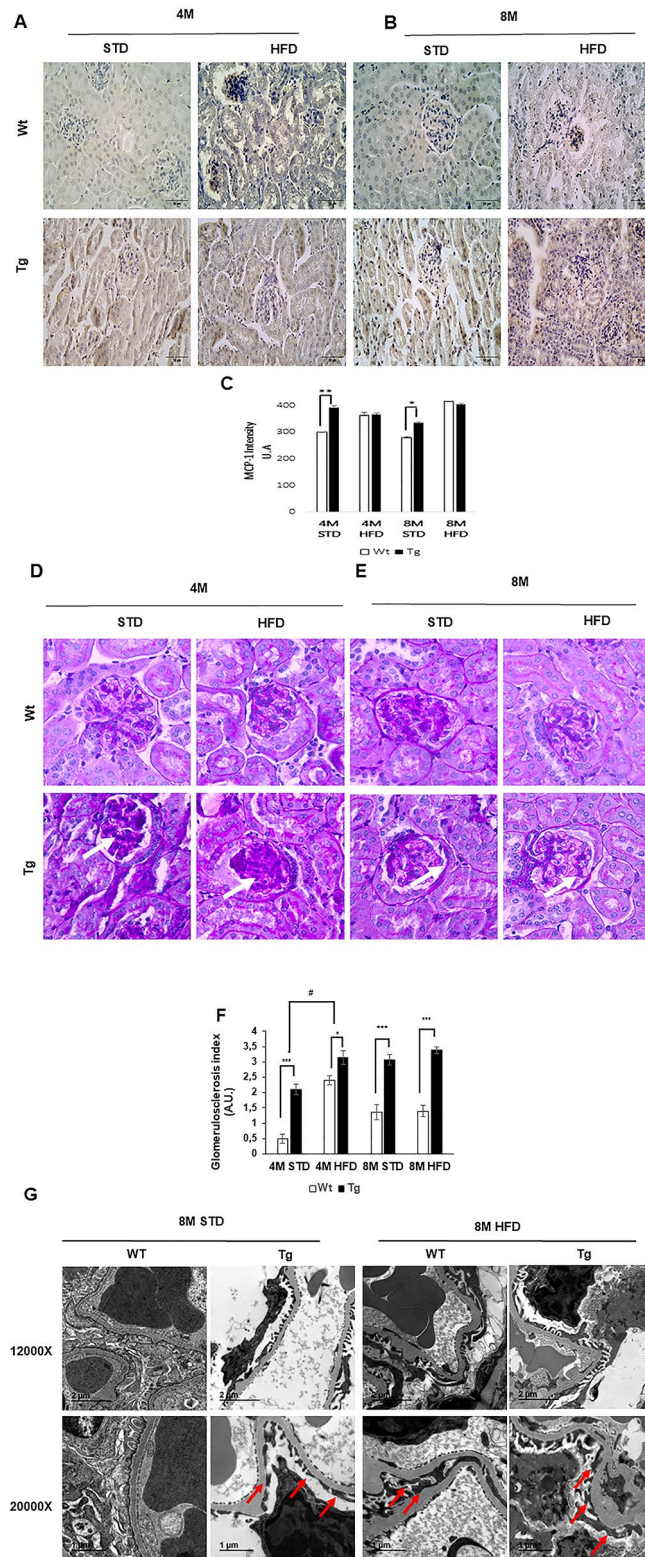


**Fig. 5.** Inflammation and damage kidney detection. A, B: MCP-1 levels were measured by immunohistochemistry in 4 M and 8M TgIAPP and Wt mice. D, E: Glomerulosclerosis index. The plots (C, F) indicate the mean and standard error is represented (n (mice number) = 4–7). \*:  $p < 0,05$ ; \*\*:  $p < 0,01$ ; \*\*\* $p < 0,005$ , \*\*\*\*  $p < 0,0005$ ). The arrows in Fig. 3D and E indicates the glomerulosclerotic regions in the TgIAPP mouse model. G: Electron microscopy of the kidney of TgIAPP and Wt of 8 M at STD and HFD conditions. Red arrows point to the effaced foot processes.

### mTORC1 pathway and ER-stress are altered in the kidney of Tg $\beta$ APP mice

mTORC1 gathers signals coordinating the presence of nutrients and growth factors availability, being disrupted in diabetic nephropathy<sup>24</sup>. In the present study, we have observed that at 4 M of age, there were no changes in mTORC1 signaling activation, as indicated by the phosphorylation of its direct target, p70S6K, when comparing Tg $\beta$ APP with WT mice. However, at older stages (8 M), there was an increase in the phosphorylation state of p70S6K, indicating an increase in mTORC1 activity, particularly in the Tg $\beta$ APP under HFD mice (Fig. 6A and B). Since, mTORC1 is one of the main regulators of ER-stress<sup>25</sup>, we analyzed the resident chaperone Bip protein. It was observed that Tg 4 M mice, fed with either STD or HFD conditions, presented an increase in Bip levels compared to their WT. However, at 8 M there was a decrease in Bip protein levels (Fig. 6A and C), suggesting that ER stress may decrease with age.

### Mitochondrial dynamics is affected in the kidney of Tg $\beta$ APP mice

Regarding mitochondrial dynamics, mitochondria undergo two dynamic processes, fusion and fission, which regulate their function and adaptation to the metabolic state of the organism<sup>26</sup>. Although we observed an increase in Mfn1 levels in Tg $\beta$ APP mice at 4 M (Fig. 7A and B), we did not observed changes in Mfn2 (Fig. 7A and C). Importantly, we noticed that in the Tg $\beta$ APP mice fed with either STD or HFD, there was a reduction in the phosphorylation status of DRP1 protein compared to their corresponding controls (Fig. 7A and D). However, in the Tg $\beta$ APP mice at 8 M, fed with either STD or HFD, there was an increase in the phosphorylation state of DRP1 compared to control mice (Fig. 7A and D). Overall, comparing the Tg $\beta$ APP 8 M mice with the Tg $\beta$ APP 4 M mice, there is a reduction in phospho-DRP1 and an increase in MFN1 and in MFN2 in both STD and HFD (Fig. 7). This data suggests a transition in mitochondrial dynamics from a predominantly fusion state at 4 M in the Tg $\beta$ APP mice to a more fissioned state in the Tg $\beta$ APP 8 M mice

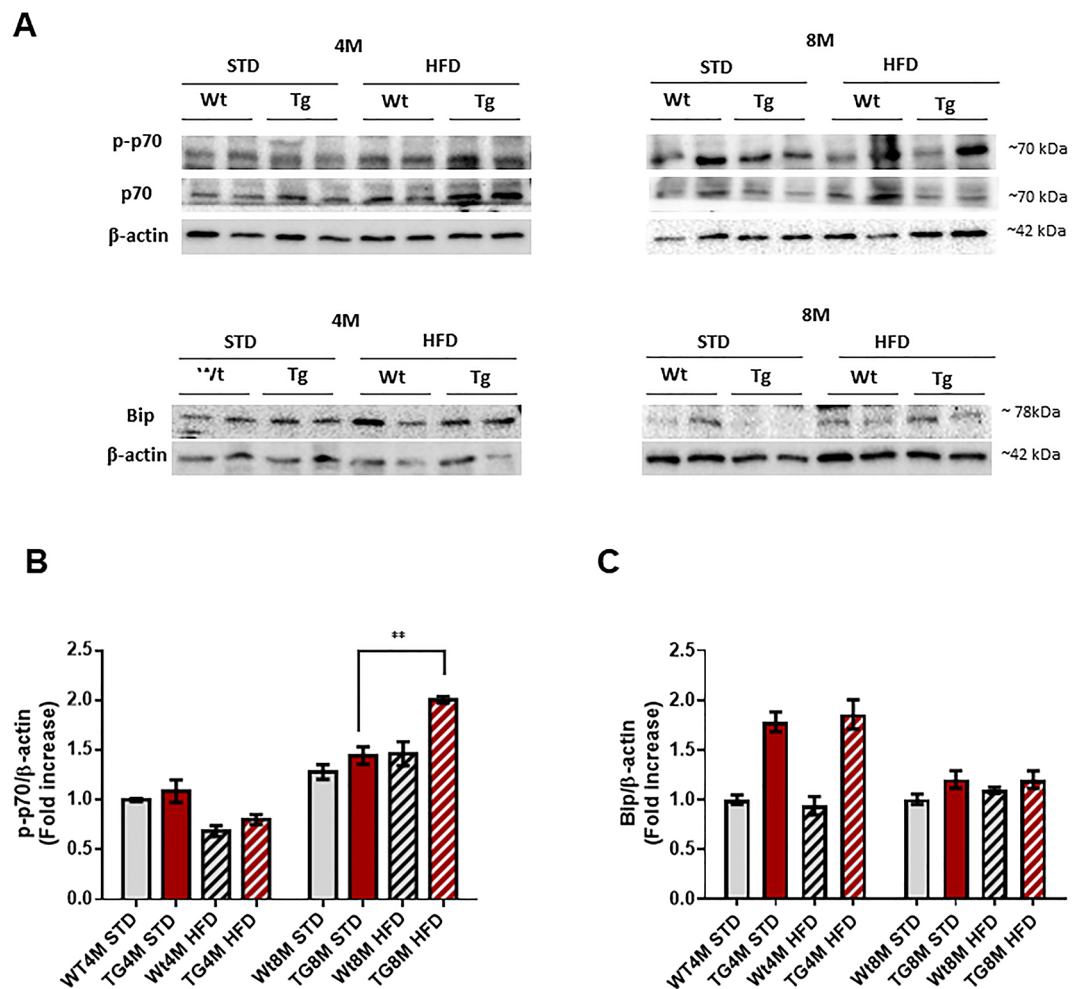


**Fig. 6.** Analysis of the mTORC1 and ER pathway of the whole kidney tissue. Western blotting was used to measure the levels of p-p70 (B), one of the main targets of mTORC1, and Bip (C), a chaperone whose levels increase under ER conditions. The plots indicate the mean and standard error is represented (n (mice number) = 4–7).

## Discussion

IAPP is a peptide mainly synthesized by the pancreas and co-secreted along with insulin. In certain species and under certain pathological conditions such as T2DM, IAPP could aggregate and form amyloid plaques like the human isoform (hIAPP)<sup>27</sup>. During the progression of T2DM, there are processes that promote hIAPP aggregation, such as reticulum overload and alterations in the insulin-amylin ratio in the secretory granules, among others. These aggregates present cytotoxic effects that include disruption of lipid membranes, generation of ROS and induction of apoptosis<sup>28</sup>.

A previous study from our group established that pancreatic  $\beta$ -cells are capable of secreting amylin internalized into extracellular vesicles as an additional mechanism of hIAPP clearance. This contributes to the elimination of hIAPP and helps to avoid its deleterious consequences

<sup>13</sup>. In this current study, we have demonstrated that mesangial, tubular and podocyte cells can take up amylin from  $\beta$ -cells, and aggregate inside these recipient cells. This result was crucial in establishing a possible link between  $\beta$ -cell and kidney cells. On the other hand, it has been previously described that some patients with diabetic nephropathy (DN) have IAPP deposits in the kidneys<sup>16</sup>. Considering these results, we decided to study the kidneys of Tg mice to hIAPP in a diabetic context induced by HFD. Using this transgenic mouse treated with HFD, we observed a time-dependent progression of glucose intolerance and insulin resistance. We have determined the accumulation of amylin in the kidney in the glomerular and periglomerular area using immunohistochemistry. Although this accumulation of amylin was clear at 4 M in the TghIAPP, at 8 M, there was a decrease in IAPP levels compared to TghIAPP 4 M mice. At the same time, TghIAPP mice 8 M under HFD were only positive for Congo Red staining, which indicates the aggregation of amylin. We interpret this paradoxical effect observed in amylin staining, as the TghIAPP 8 M mice may have lower levels of monomeric IAPP because this protein might be aggregating and the antibody we used, only detects the soluble form of amylin. As mentioned above, hIAPP is the isoform that can fold into aggregates. This aggregation process follows a sigmoidal kinetic where lower levels of monomeric hIAPP could be due to the initiation of this aggregation process<sup>29</sup>. In the process of amylin aggregate formation, previously formed oligomers serve as nucleation sites for the assembly of larger oligomers and pre-fibrillar structures, resulting in the disappearance of smaller oligomers. This observation aligns with our findings: in the TghIAPP mouse model fed with HFD, only oligomers were detected at 4 months of age, whereas at 8 months, only mature aggregates were present.

It is known that amylin can deposit in the mesangial area and is able to thicken Bowman's capsule in patients with diabetic nephropathy<sup>16</sup>. However, these changes are produced by the extracellular form of amylin, which is freely transported in the bloodstream. In this study, however, we propose that the deleterious effects of amylin are generated within the kidney cells, because of its capacity to be incorporated into the cells in an endocytic-dependent manner, as it has been previously observed<sup>13</sup>.

Inflammation is a key factor in the development and progression of T2DM and consequently DN<sup>30</sup>. MCP-1 is a specific chemokine that recruits monocytes to the site of inflammation. Levels of this chemokine have been correlated with many glomerulopathies<sup>31,32</sup>. Another study reported that MCP-1 may contribute to the initiation and progression of DN<sup>33</sup>. In addition, treatment with anti-MCP-1 antibodies reduces glomerulosclerosis<sup>34</sup>. All these results support the role of MCP-1 in DN. Our results show that both TghIAPP at 4 M and 8 M mice under the STD diet had higher levels of this inflammatory protein compared to WT. However, in mice fed HFD there is no difference between Tg and Wt. These results suggest that HFD is the main factor by which the levels of this protein increase, regardless of the genotype. In this regard, HFD has been shown to increase circulating MCP-1 levels in Wistar rats<sup>35</sup>, as well as in neutrophils<sup>36</sup>.

On the other hand, it is interesting that TghIAPP 4 M and 8 M under the STD diet showed higher levels of MCP-1 in comparison with their corresponding controls and increased levels of caspase-1 in the TghIAPP at 8 M. These results suggest that in a non-proinflammatory situation, a higher inflammation can be detected in the TghIAPP than in WT mice. As it was previously mentioned, glomerulosclerosis is a hallmark of DN and renal damage. In our study we found that all TghIAPP mice had an increased glomerulosclerosis index compared to WT mice. This is very important since it has been previously described that DN patients with IAPP deposition in the kidney had more severe glomerulosclerosis than those without IAPP deposition<sup>16</sup>. In addition, TghIAPP 4 M HFD mice showed a significant increase in the glomerulosclerosis index compared to TghIAPP 4 M STD mice. Also, TghIAPP 4 M HFD mice have significant higher levels of IAPP than TghIAPP 4 M STD mice. However, TghIAPP 8 M STD mice show a similar glomerulosclerosis index to TghIAPP 8 M HFD mice. Furthermore, these two groups of mice have similar levels of IAPP. Therefore, it is suggested that the increase in the glomerulosclerosis index may be associated with IAPP deposition in the kidney.

Additionally, we observed the emergence of foot effacing processes in podocytes of TghIAPP 8 M mice under STD conditions, as well as in both WT and TghIAPP mice under HFD conditions, as evidenced by electron microscopy. This finding is of significant importance since transgenic TghIAPP mice under STD conditions exhibit damage similar to that observed in mice under a HFD, underscoring the role of hIAPP in the injury to these cells. Podocytes play a crucial role in renal physiology, and their injury has been recognized as a pivotal event leading to glomerulosclerosis and loss of renal function.

To establish the consequences of the increased IAPP deposits and the presence of hIAPP aggregates in the TghIAPP mice, we decided to study some signalling pathways that are disrupted in situations of diabetic nephropathy (DN) *in vitro* and *in vivo*. Regarding this, we studied mTORC1, ER stress and mitochondrial dynamics. We also, evaluated kidney damage by analysing glomerulosclerosis index and inflammation. mTORC1 is a kinase that regulates fundamental processes for cell homeostasis such as protein synthesis and autophagy. This pathway is disrupted in several tissues involved in the development and progression of T2DM. In pancreas, the activity of this kinase is fundamental in the first stage of the disease to increase in insulin production. However, a chronic activation of this pathway is detrimental to  $\beta$  cells [2].

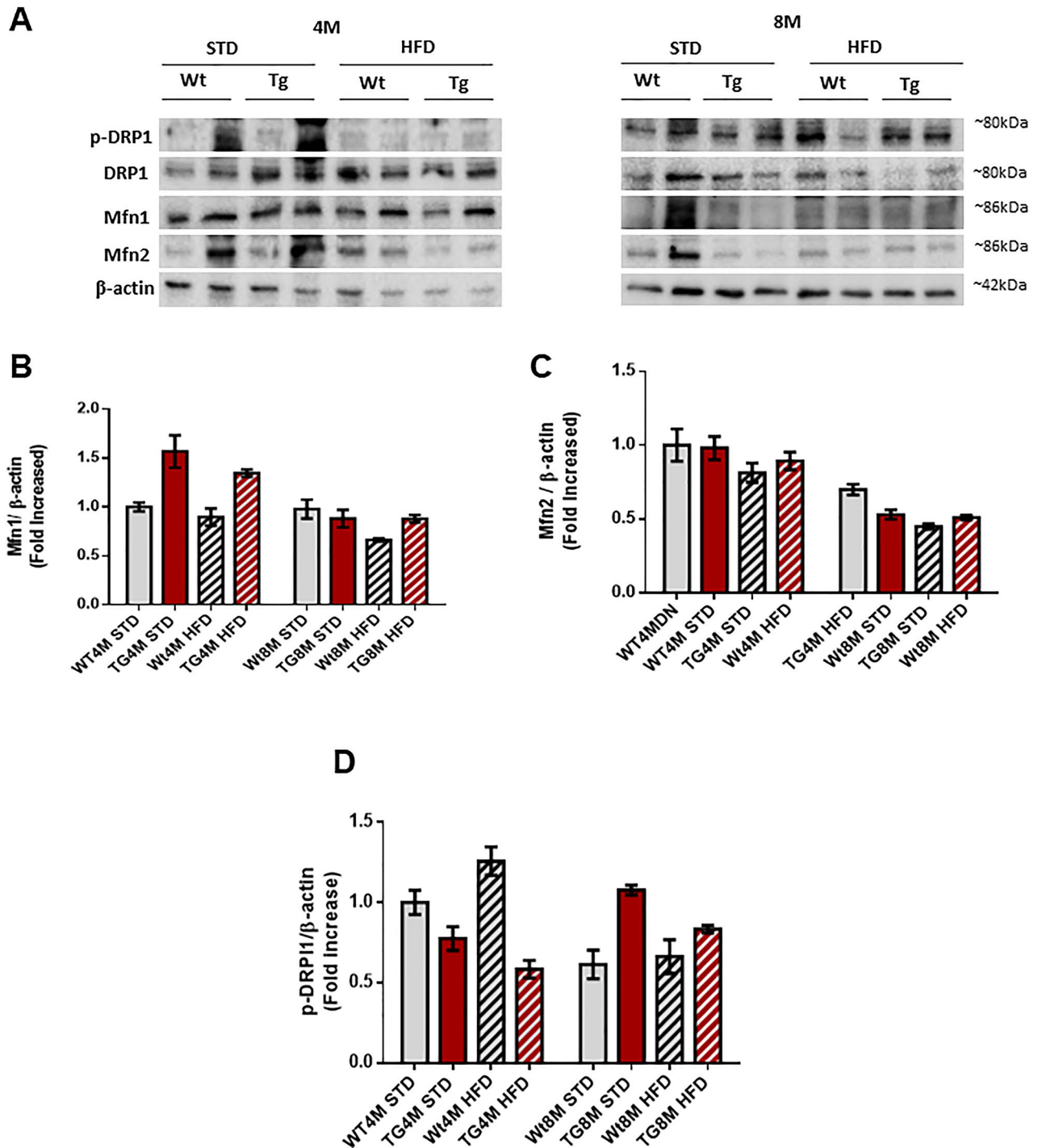


**Fig. 7.** Analysis of mitochondria dynamics of the whole kidney tissue. Western Blotting quantification of different proteins involved in mitochondria fusion and fission. The plots indicate the mean and standard error is represented ( $n$  (mice number) = 4–7). A: Western Blot images B, C, D: plots of Mfn1, Mfn2, p-DRP1 respectively.

Regarding mTORC1 pathway, our findings revealed that mesangial and tubular cells exposed to conditioned medium for 8 and 24 h exhibited a reduction in mTORC1 activation, as evidenced by decreased levels of p-ULK1 (757) and p-p70. This reduction was particularly significant in mesangial cells at 24 h. These results are likely linked to the observed elevation in p-PERK and Bip. It is evident that cells harbouring amylin aggregates experience a notable increase in ER stress, which triggers the unfolded protein response (UPR). This UPR leads to elevated levels of Bip and p-PERK, while simultaneously reducing protein synthesis, thereby inhibiting the mTORC1 pathway<sup>37</sup>. This adaptive mechanism enables the cell to respond to damage, as inhibition of mTOR has been demonstrated to enhance cell viability under ER stress conditions<sup>38</sup>.



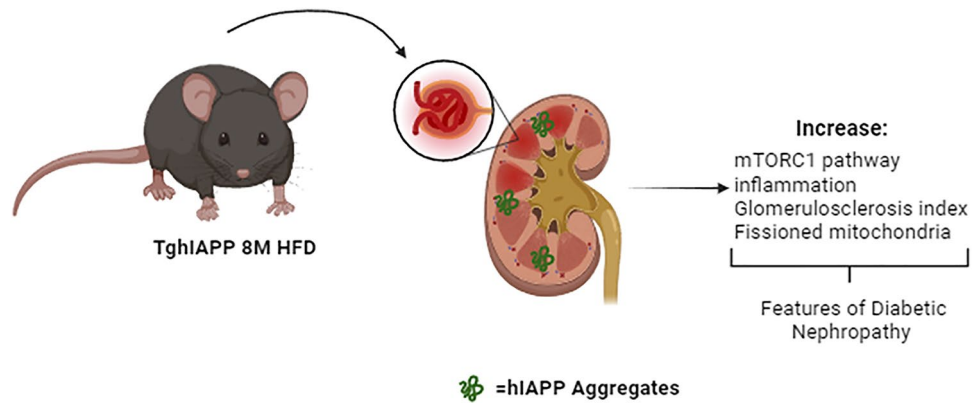


**Fig. 8.** Scheme of the main results. This work shows for the first time the pathological role of hIAPP, which has been found to be deposited in the kidneys of ND patients. TghIAPP 8 M mice treated with HFD exhibit hIAPP aggregates and an increased in mTORC1 signaling pathway, inflammation, and altered mitochondrial dynamics.

Moreover, this cellular adaptation mechanism prevents cells from undergoing apoptosis, as evidenced by the absence of changes in Bcl-xL and cleaved caspase-3 levels in mesangial and tubular cells, respectively. It is apparent that ER stress can lead to two outcomes: either attempting to resolve the issue or triggering cell death. In this scenario, the cell responds downregulating protein synthesis via mTORC1, thereby averting cell death<sup>38</sup>. However, chronic ER stress may paradoxically elevate mTOR activity, as will be further elucidated in the subsequent *in vivo* model analysis.

On the other hand, podocytes exhibit an increase in ER stress at 8 h, accompanied by elevated levels of cleaved caspase-3, rendering them more susceptible to acute damage. However, by 24 h, they seem to recover and manage this damage effectively, indicated by a decrease in Bip and cleaved caspase-3 levels. Thus, it is evident that mesangial and tubular cells display higher ER stress compared to podocytes. However, mitochondrial dynamics appear to be more significantly affected in podocytes than in mesangial and tubular cells, as will be discussed further.

In the *in vivo* model, we did not find any difference in all 4 M mice, neither between genotypes nor between diets. It is described that mTORC1 activation is associated with aging<sup>39</sup>. Then, if we compare the groups only by their ages, we found an increase in the activation of this pathway in 8 M compared with 4 M mice in both genotypes. When we compare 8 M mice only considering their diet, we found that mice fed with HFD had high levels of p-p70 in both Wt and Tg. It is well established that HFD induce an activation of mTORC1, as well as insulin resistance<sup>40</sup>. In addition, an increase in the phosphorylation status of p70 was also observed in Tg 8 M HFD mice, which is the only group showing amyloid aggregates, suggesting a relationship between this signalling pathway and the presence of hIAPP aggregates. In Alzheimer's disease, it has been established a concomitant increase in the activation of mTOR and A $\beta$  deposition. Regarding this, previous studies have shown that mTOR signalling was abnormally upregulated after direct injection of A $\beta$  oligomers into mouse hippocampus. Besides, it has been described that mTOR hyperactivation can enhanced both A $\beta$  generation and deposition<sup>41</sup>. Although Tg 8 M mice present a slight increase in the levels of Bip chaperone, an indicator of ER-stress, compared to Wt. The increase in Bip may initially be due to activation of the unfolded protein response (UPR), which induces chaperone synthesis to deal with the accumulation of proteins. However, prolonged ER-stress can promote apoptosis through an inhibition of Bip expression<sup>42</sup>. This could be operating in the TghIAPP 8 M mice, which could justify the reduction in Bip levels, compared to 4 M Tg mice.

Mitochondrial status is necessary for insulin secretion, under sustained conditions of hyperglycemia mitochondria increase the production of reactive oxygen species (ROS), which contribute and exacerbates the microvascular complications of T2DM such as nephropathy. This is why the homeostasis of this organelle is fundamental for maintaining a correct cellular state. Mitochondria undergo fusion and fission processes to adapt to the energetic state and protect themselves against damage, either by exchanging components when fusing or by secreting damaged mitochondria when fission<sup>43</sup>.

*In vitro* studies revealed no significant alterations in mitochondrial dynamics; however, there was a tendency for Mfn1 levels to decrease across all types of kidney cells, suggesting a potential initiation of the fission process. This decrease in Mfn1 and Mfn2 is only significant for podocytes, demonstrating greater impairment of mitochondrial dynamics in podocytes compared to mesangial and tubular cells.

We demonstrate how TghIAPP mice have altered mitochondrial dynamics at both 4 M and 8 M mice. Firstly, no significant differences were found between neither mouse fed with HFD diet versus STD. However, it was observed that Tg 4 M mice showed a fused mitochondrial state, represented by a reduction in the phosphorylation state of DRP1 levels and a concomitant increase in MFN1 protein level. This result could indicate a compensatory mechanism of mitochondria, in which they protect themselves from damage by combining components of their mitochondrial matrix. In fact, it has been previously described that, in the early stages of DN, mitochondria tend to a fused state<sup>44</sup>. In contrast, Tg 8 M mice exhibited a more fissioned mitochondrial state compared to their respective controls, with no difference between diets. Besides, we did not find any difference between 4 M



and 8 M Wt mice. Therefore, age may not be playing a role in the mitochondrial dynamics switch observed between 4 M and 8 M mice. This change in mitochondrial dynamics could be due to the fact that in the TghIAPP 8 M mice have a higher damage. In this case mitochondria tend to a fissioned state to subsequently be either eliminated by mitophagy or to promote apoptosis if the cellular state requires it, as it has been suggested before<sup>45</sup>. Studies on DN in both patients and rodents have shown that a fissioned mitochondrial state is associated with markers of renal damage<sup>46</sup>. In addition, silencing genes essential for fission, such as DRP1, has been reported to protect against the development of DN in rodents<sup>47</sup>.

In summary, we report that renal cells (podocytes, mesangial and tubular cells), can take up hIAPP coming from  $\beta$ -cells and have aggregates of this protein inside them. On the other hand, we have shown for the first time hIAPP aggregates in the kidney of TghIAPP mice. In addition,

these TghIAPP mice have shown more levels of MCP-1, caspase 1 and glomerulosclerosis index and disruption in some proteins involved in mTORC1 pathway, mitochondria dynamics and ER-stress. Although our experimental model using both in vitro as well as in vivo approaches indicates that overexpressing human amylin is deleterious for kidney cells, it is necessary to corroborate these data using type 2 diabetic patients. In Fig. 8, it is resumed the main findings obtained in the present manuscript both in vitro as well as in vivo.

## Data availability

The datasets analysed during the current study are available from the corresponding author on reasonable request.

Received: 23 July 2024; Accepted: 18 October 2024

Published online: 21 October 2024

## References

- James, D. E., Stöckli, J. & Birnbaum, M. J. The aetiology and molecular landscape of insulin resistance. *Nat. Rev. Mol. Cell. Biol.* **22**, 751–771 (2021).
- Guillén, C. & Benito, M. mTORC1 overactivation as a key aging factor in the progression to type 2 diabetes Mellitus. *Front. Endocrinol. (Lausanne)*. **9**, 621 (2018).
- Bartolomé, A. et al. Pancreatic  $\beta$ -cell failure mediated by mTORC1 hyperactivity and autophagic impairment. *Diabetes*. **63**, 2996–3008 (2014).
- Bartolomé, A., Guillén, C. & Benito, M. Autophagy plays a protective role in endoplasmic reticulum stress-mediated pancreatic  $\beta$  cell death. *Autophagy*. **8**, 1757–1768 (2012).
- Bugliani, M. et al. Modulation of autophagy influences the function and survival of human pancreatic beta cells under endoplasmic reticulum stress conditions and in type 2 diabetes. *Front. Endocrinol.* **10**, 52 (2019).
- Ebato, C. et al. Autophagy is important in islet homeostasis and compensatory increase of beta cell mass in response to high-fat diet. *Cell. Metab.* **8**, 325–332 (2008).
- Bhansali, S., Bhansali, A., Walia, R., Saikia, U. N. & Dhawan, V. Alterations in mitochondrial oxidative stress and mitophagy in subjects with prediabetes and type 2 diabetes mellitus. *Front. Endocrinol.* **8**, 347 (2017).
- Westermarck, P., Andersson, A. & Westermarck, G. T. Islet amyloid polypeptide, islet amyloid, and diabetes mellitus. *Physiol. Rev.* **91**, 795–826 (2011).
- Haataja, L., Gurlo, T., Huang, C. J. & Butler, P. C. Islet amyloid in type 2 diabetes, and the toxic oligomer hypothesis. *Endocr. Rev.* **29**, 303–316 (2008).
- Costes, S., Gurlo, T., Rivera, J. F. & Butler, P. C. UCHL1 deficiency exacerbates human islet amyloid polypeptide toxicity in  $\beta$ -cells: evidence of interplay between the ubiquitin/proteasome system and autophagy. *Autophagy*. **10**, 1004–1014 (2014).
- Rivera, J. F., Costes, S., Gurlo, T., Glabe, C. G. & Butler, P. C. Autophagy defends pancreatic  $\beta$  cells from human islet amyloid polypeptide-induced toxicity. *J. Clin. Invest.* **124**, 3489–3500 (2014).
- García, M. et al. Pancreatic  $\beta$  cells overexpressing hIAPP impaired mitophagy and unbalanced mitochondrial dynamics. *Cell. Death Disease*. **9**, 481 (2018).
- Burillo, J. et al. Human amylin aggregates release within exosomes as a protective mechanism in pancreatic  $\beta$  cells: pancreatic  $\beta$ -hippocampal cell communication. *Biochim. Biophys. Acta Mol. Cell. Res.* **1868**, 118971 (2021).
- Pelle, M. P. et al. Up-Date on diabetic nephropathy. *Life*. **12**, 1202 (2022).
- Verma, N. & Despa, F. The association between renal accumulation of pancreatic amyloid-forming amylin and renal hypoxia. *Front. Endocrinol.* **14**, 1104662 (2023).
- Gong, W. et al. Amylin deposition in the kidney of patients with diabetic nephropathy. *Kidney Int.* **72**, 213–218 (2007).
- Verma, N. et al. Diabetic microcirculatory disturbances and pathologic erythropoiesis are provoked by deposition of amyloid-forming amylin in red blood cells and capillaries. *Kidney Int.* **97**, 143–155 (2020).
- Soty, M. et al. Involvement of ATP-densitive potassium (KATP) channels in the loss of beta-cell function induced by human islet amyloid polypeptide. *J. Biol. Chem.* **286**, 40857–40866 (2011).
- Janson, J. et al. Spontaneous diabetes mellitus in transgenic mice expressing human islet amyloid polypeptide. *Proc. Natl. Acad. Sci. USA*. **93**, 7283–7288 (1996).
- Staderini, M. et al. A fluorescent styrylquinoline with combined therapeutic and diagnostic activities against Alzheimer's and prion diseases. *ACS Med. Chem. Lett.* **4**, 225–229 (2013).
- Martínez-García, C. et al. Accelerated renal disease is associated with the development of metabolic syndrome in a glucolipotoxic mouse model. *Dis. Model. Mech.* **5**, 636–648 (2012).
- Mallipattu, S. K. & He, J. C. A new mechanism for albuminuria-induced podocyte injury. *J. Am. Soc. Nephrol.* **24**, 1709–1711 (2013).
- Viana-Huete, V. et al. Male brown fat-specific double knockout of IGF1R/IR: atrophy, mitochondrial fission failure, impaired thermogenesis, and obesity. *Endocrinology*. **159**, 323–340 (2018).
- Yasuda-Yamahara, M., Kume, S. & Maegawa, H. Roles of mTOR in Diabetic kidney disease. *Antioxidants*. **10**, 321 (2021).
- Cunard, R. Endoplasmic reticulum stress in the diabetic kidney, the good, the bad and the ugly. *J. Clin. Med.* **4**, 715–740 (2015).
- Tilokani, L., Nagashima, S., Paupe, V. & Prudent, J. Mitochondrial dynamics: overview of molecular mechanisms. *Essays Biochem.* **62**, 341–360 (2018).
- Lutz, T. A. Creating the amylin story. *Appetite*. **172**, 105965 (2022).
- Raleigh, D., Zhang, X., Hastoy, B. & Clark, A. The  $\beta$ -cell assassin: IAPP cytotoxicity. *J. Mol. Endocrinol.* **59**, R121–R140 (2017).
- Saghir, A., El, Farrugia, G. & Vassallo, N. The human islet amyloid polypeptide in protein misfolding disorders: mechanisms of Aggregation and Interaction with biomembranes. *Chem. Phys. Lipids*. **234**, 105010 (2021).
- Duran-Salgado, M. B. & Rubio-Guerra, A. F. Diabetic nephropathy and inflammation. *World J. Diabetes*. **5**, 393–398 (2014).

31. Rovin, B. H., Doe, N. & Tan, L. C. Monocyte chemoattractant protein-1 levels in patients with glomerular disease. *Am. J. Kidney Dis.* **27**, 640–646 (1996).
32. Brown, Z., Robson, R. L. & Westwick, J. Regulation and expression of chemokines: potential role in glomerulonephritis. *J. Leukoc. Biol.* **59**, 75–80 (1996).
33. Banba, N. et al. Possible relationship of monocyte chemoattractant protein-1 with diabetic nephropathy. *Kidney Int.* **58**, 684–690 (2000).
34. Wada, T. et al. Intervention of crescentic glomerulonephritis by antibodies to monocyte chemotactic and activating factor (MCAF/MCP-1). *FASEB J.* **10**, 1418–1425 (1996).
35. Syarif, Rasyid, H., Aman, M. & Lawrence, G. S. High-fat diet increases the level of circulating Monocyte chemoattractant Protein-1 in Wistar rats, independent of obesity. *Ann. Med. Surg.* **65**, 102266 (2021).
36. Osaka, M. et al. Critical role of the C5a- activated neutrophils in high-fat diet-induced vascular inflammation. *Sci. Rep.* **6**, 21391 (2016).
37. Guan, B. J. et al. Translational control during endoplasmic reticulum stress beyond phosphorylation of the translation initiation factor eIF2 $\alpha$ . *J. Biol. Chem.* **289**, 12593–12611 (2014).
38. Hofmann, C. et al. mTORC1 inhibition impairs activation of the unfolded protein response and induces cell death during ER stress in cardiomyocytes. *Am. J. Physiol. Heart Circ. Physiol.* **325**, H311–H320 (2023).
39. Mannick, J. B. & Lammung, D. W. Targeting the biology of aging with mTOR inhibitors. *Nat. Aging.* **3**, 642–660 (2023).
40. McIver, C. M., Wycherley, T. P. & Clifton, P. M. mTOR signaling and ubiquitin-proteasome gene expression in the preservation of fat free mass following high protein, calorie restricted weight loss. *Nutr. Metab.* **9**, 83 (2012).
41. Querfurth, H. & Lee, H.-K. Mammalian/mechanistic target of rapamycin (mTOR) complexes in neurodegeneration. *Mol. Neurodegener.* **16**, 44 (2021).
42. López, I. et al. p53-mediated suppression of BiP triggers BIK-induced apoptosis during prolonged endoplasmic reticulum stress. *Cell. Death Differ.* **24**, 1717–1729 (2017).
43. Rovira-Llopis, S. et al. Mitochondrial dynamics in type 2 diabetes: pathophysiological implications. *Redox Biol.* **11**, 637–645 (2017).
44. Coughlan, M. T. et al. Mapping time-course mitochondrial adaptations in the kidney in experimental diabetes. *Clin. Sci.* **130**, 711–720 (2016).
45. Forbes, J. M. & Thorburn, D. R. Mitochondrial dysfunction in diabetic kidney disease. *Nat. Rev. Nephrol.* **14**, 291–312 (2018).
46. Zhan, M., Brooks, C., Liu, F., Sun, L. & Dong, Z. Mitochondrial dynamics: regulatory mechanisms and emerging role in renal pathophysiology. *Kidney Int.* **83**, 568–581 (2013).
47. Ayanga, B. A. et al. Dynamin-Related protein 1 Deficiency improves mitochondrial fitness and protects against Progression of Diabetic Nephropathy. *J. Am. Soc. Nephrol.* **27**, 2733–2747 (2016).

## Acknowledgements

We thank Programa Investigo for funding Carlos González-Blanco, and Elena González for her assistance in the laboratory. We thank the immunofluorescence facility core from the Complutense University of Madrid for their technical assistance. Rat insulinoma cell line INS1E were kindly provided by P. Maechler (Université de Genève, Geneva, Switzerland); INS1E overexpressing human amylin (INS1E-hIAPP) were generously supplied by Anna Novials (IDIBAPS, Barcelona, Spain).

## Author contributions

The individual role of all the authors in the present manuscript are the following: Conceptualization, C.G.; methodology, S. I-F, C. G-B., A. G-C, A. I-L, G.G; software, C.G., S. I-F, A. G-C, A.I-L.; validation, C.G, S. I-F, A. G-C, A.I-L.; formal analysis, C.G., S. I-F, A. G-C., A. I-L.; investigation, S. I-F, G.G, A. G-C., A.I-L.; resources, G.G.; data curation, C.G.; writing—original draft preparation, C.G., S I-F, A G-C, A.I-L; writing—review and editing, S.I-F, C.G-B., A.G-C., A.I-L., G.G., A.G-A., A.L., O.P, G.M-G., M.B., C.G.; visualization, C.G., S.I-F, A.G-C., A.I-L; supervision, C.G., G.G.; project administration, C.G.; funding acquisition, C.G., M.B. All authors have read and agreed to the published version of the manuscript.

## Funding

This work was supported by grants PID2020-113361RB-I00 funded by MICIN/AEI/FEDER, EU C. Guillén and M. Benito and Spanish Diabetes and Associated Metabolic Research Network (CIBERdem) to C. Guillén. We thank to P2022/BMD-7227, MOIR-ACTOME-CM. Dirección General de Investigación e Innovación Tecnológica (DGIIT). Consejería de Educación y Universidades. Comunidad de Madrid. Madrid, España.

## Declarations

### Competing interests

The authors declare no competing interests.

### Additional information

**Supplementary Information** The online version contains supplementary material available at <https://doi.org/10.1038/s41598-024-77063-9>.

**Correspondence** and requests for materials should be addressed to C.G.

**Reprints and permissions information** is available at [www.nature.com/reprints](http://www.nature.com/reprints).

**Publisher's note** Springer Nature remains neutral with regard to jurisdictional claims in published maps and institutional affiliations.

**Open Access** This article is licensed under a Creative Commons Attribution-NonCommercial-NoDerivatives 4.0 International License, which permits any non-commercial use, sharing, distribution and reproduction in any medium or format, as long as you give appropriate credit to the original author(s) and the source, provide a link to the Creative Commons licence, and indicate if you modified the licensed material. You do not have permission under this licence to share adapted material derived from this article or parts of it. The images or other third party material in this article are included in the article's Creative Commons licence, unless indicated otherwise in a credit line to the material. If material is not included in the article's Creative Commons licence and your intended use is not permitted by statutory regulation or exceeds the permitted use, you will need to obtain permission directly from the copyright holder. To view a copy of this licence, visit <http://creativecommons.org/licenses/by-nc-nd/4.0/>.

© The Author(s) 2024